



# Predicting of the Quality Attributes of Orange Fruit Using Hyperspectral Images

V. Aredo<sup>1</sup>, L. Velásquez<sup>1</sup>, J. Carranza-Cabrera<sup>2</sup>, R. Siche<sup>2,3\*</sup>✉

1. Food Engineering Graduate Program, Faculty of Animal Science and Food Engineering, University of São Paulo (USP), Pirassununga, São Paulo, 13635-900, Brazil

2. Facultad de Ciencias Agropecuarias, Universidad Nacional de Trujillo. Av. Juan Pablo II s/n. Ciudad Universitaria, Trujillo, Peru

3. Universidad Señor de Sipán, km 5 Carretera a Pimentel, Chiclayo, Peru

## HIGHLIGHTS

- Full models for internal quality attributes of orange fruits had low performance.
- Full models for external quality attributes presented a high performance for L\*, a\*, b\*, and color index.
- The simplified models presented similar performance to those obtained for external quality attributes.
- Hyperspectral reflectance imaging has potential for predicting color of oranges in an objective and noncontact way.

## Article type

Original article

## Keywords

Spectrum Analysis  
Citrus  
Quality Control  
Food Technology

## Article history

Received: 1 May 2019

Revised: 17 Jul 2019

Accepted: 25 Jul 2019

## Acronyms and abbreviations

CI=Color Index  
 $R^2_c$ =Coefficient of determination of calibration  
 $R^2_p$ =Coefficient of determination of prediction  
ROI=Region of Interest  
SEC=Standard Error of Calibration  
SEP=Standard Error of Prediction  
TA=Titrateable Acidity  
TSS=Total Soluble Solids

## ABSTRACT

**Background:** Hyperspectral image analysis is a fast and non-destructive technique that is being used to measure quality attributes of food products. This research investigated the feasibility of predicting internal quality attributes, such as Total Soluble Solids (TSS), pH, Titrateable Acidity (TA), and maturity index (TSS/TA); and external quality attributes such as color components (L\*, a\*, b\*) as well as Color Index (CI) of Valencia orange fruit using hyperspectral reflectance imaging in the range of 400-1000 nm.

**Methods:** Oranges were scanned by the system in order to build full models for predicting quality attributes using partial least squares regression. Optimal wavelengths were identified using the regression coefficients from full models, which were used to build simplified models by multiple linear regression. The coefficient of determination of prediction ( $R^2_p$ ) and the Standard Error of Prediction (SEP) were used to measure the performance of the models obtained.

**Results:** Full models for internal quality attributes had low performance ( $R^2_p < 0.3$ ,  $SEP > 50\%$ ). Full models for external quality attributes presented a high performance for L\* ( $R^2_p = 0.898$ ,  $SEP = 19\%$ ), a\* ( $R^2_p = 0.952$ ,  $SEP = 13\%$ ), b\* ( $R^2_p = 0.922$ ,  $SEP = 20\%$ ), and CI ( $R^2_p = 0.972$ ,  $SEP = 12\%$ ). The simplified models presented similar performance to those obtained for external quality attributes.

**Conclusion:** Hyperspectral reflectance imaging has potential for predicting color of oranges in an objective and noncontact way.

© 2019, Shahid Sadoughi University of Medical Sciences. This is an open access article under the Creative Commons Attribution 4.0 International License.

## Introduction

The quality of the fresh fruit is defined by a series of external attributes that determine their suitability for the consumer (Saldaña et al., 2014). These attributes can

include size, weight, shape, color, or absence of defects, which in turn are used to sort the fruit manually or automatically. In addition, internal quality attributes, such as

\* Corresponding author. ✉ rsiche@unitru.edu.pe  
ORCID ID: <https://orcid.org/0000-0003-3500-4928>

**To cite:** Aredo V., Velásquez L., Carranza-Cabrera J., Siche R. (2019). Predicting of the quality attributes of orange fruit using hyperspectral images. *Journal of Food Quality and Hazards Control*. 6: 82-92.

firmness, water content, soluble solids content, pH, and titratable acidity are also very important in the modern food industry (Siche et al., 2016). Instrumental techniques to measure these attributes can be destructive or involve a considerable amount of manual labor, which is slow, costly, and subject to human error and inconsistencies (Barreto et al., 2018). Therefore, accurate, reliable, and nondestructive systems are needed to examine automatically the products.

In this sense, hyperspectral imaging has emerged as a promising technology in the food quality assurance due to its precision, speed, as well as the minimum level of sample preparation (Vejarano et al., 2017). This technology that integrates spectroscopy and conventional image analysis allows the identification of different components simultaneously and the location of their spatial distribution in a sample (Orrillo et al., 2019). For these purposes, spectral data is processed through multivariate statistical methods that handle the high dimensionality and collinearity of the data to obtain quantitative models. One of these methods is the partial least squares regression, which has been widely utilized to build robust and reliable empirical predictive models for applications in food products (Aredo et al., 2017; ElMasry et al., 2007; Huang et al., 2014).

Quality attributes of different fruits have been previously assessed in some researches by hyperspectral imaging. In these studies, the reflectance mode was the most often used to obtain spectral information (Siche et al., 2016). For example, it had been used for predicting color and firmness of bananas in a spectral region of 400-1023 nm (Xie et al., 2018) and Total Soluble Solids (TSS) of apples in the spectral region of 900-1700 nm (Dong et al., 2016) and 1000-2500 nm (Zhang et al., 2019). Also, hyperspectral imaging had been applied for evaluation of TSS of kiwifruit in the spectral region of 865-1712 nm (Guo et al., 2016) and TSS, Titratable Acidity (TA), and maturity index (TSS/TA) of limes in the spectral region of 929-1671 nm (Teerachaichayut and Ho, 2017). Hence, ripeness, astringency, and firmness of persimmon in a spectral region of 450-1020 nm had been identified using hyperspectral imaging (Munera et al., 2017).

Orange is the most important commercial citrus fruit and is mainly cultivated in countries such as Brazil, China, United States, and Mexico. In 2018/2019, global orange production is expected to reach 51.8 million metric tons, with 56% of this production destined for consumption as fresh fruit (USDA, 2019). In addition, a noncontact method for measuring quality of fresh orange fruit, which allows automation of the sorting of this fruit, could decrease costs and ensure its quality.

Previously, hyperspectral reflectance imaging has been used with success in the evaluation of external quality attributes of orange fruit as the presence of common

defects as decay caused by fungus (Folch-Fortuny et al., 2016; Yin et al., 2017), infestation, canker spot, copper burn, phytotoxicity, and heterochromatic stripe (Li et al., 2011). Concerning internal quality attributes of this fruit, few hyperspectral imaging studies have been reported. For instance, the prediction of TSS by hyperspectral reflectance imaging (Guo et al., 2008) and hyperspectral laser-induced fluorescence imaging (Liu et al., 2007), and classification of maturity (period of growth from blossom) by hyperspectral diffuse transmittance imaging (Wei et al., 2017).

In order to explore a complete measurement of orange fruit quality attributes, the main goal of this study was to assess the potential of hyperspectral reflectance imaging for the prediction of TSS, pH, TA, TSS/TA, color components ( $L^*$ ,  $a^*$ ,  $b^*$ ), as well as Color Index (CI) of this fruit.

## Materials and methods

### Orange fruit samples

Orange fruit samples (*Citrus sinensis* L., Valencia variety) were collected from Rodríguez de Mendoza/Amazonas (Peru). In total, 80 samples free of undesirable characteristics such as physical damages, diseases, and polluting components were used. For a realistic application, the fruits were in a range of commercial ripeness recommended for local farmers, which was evaluated by the descriptive statistics. The samples were randomly sorted into two groups; a “calibration set” that consisted of 75% of the samples and a “prediction set” consisted of the rest of samples for external validation of models. This sampling criterion was based on studies with similar purposes in grape seeds (Rodríguez-Pulido et al., 2014), limes (Teerachaichayut and Ho, 2017), and blueberries (Leiva-Valenzuela et al., 2013).

### Hyperspectral imaging system and image acquisition

A line-scan hyperspectral imaging system in reflectance mode that acquires images in a spectral region of 400-1000 nm (Pica XC, Resonon Inc., USA) was used. Features of the system were described previously by Velásquez et al. (2017).

The image acquisition of the orange fruits was carried out with an adjusted spectral resolution of 8 nm (yielding 75 spectral bands) for a rapid acquisition and processing of images, and a primary reduction of the dimensionality and collinearity of spectral data (Aredo et al., 2017). The speed of translation stage was optimized to 0.3 cm/s for acquiring proportional images to the real dimensions of the sample. Each intact sample was imaged in the stem end facing vertically toward the camera (Leiva-

Valenzuela et al., 2013). In addition, half-orange fruits were also imaged to obtain spectral information from the pulp (Ma et al., 2018).

#### Reference measurement of quality attributes

After the acquisition of images of the samples, the reference of the quality attributes was measured. To do this, each fruit was manually squeezed and filtered to obtain juice, which was used for determination of TSS (%; method 932.12), pH (method 981.12), and TA (% citric acid; method 942.15) according to AOAC (2005). Additionally, the ratio TSS/TA was calculated for defining the maturity of orange fruit. The color measurement in CIELAB space was carried out in five random points on the orange fruit skin using a colorimeter (JZ-300, Shenzhen Kingwell Instruments Co., China), obtaining  $L^*$ ,  $a^*$ ,  $b^*$  parameters and the CI, which was calculated using the following equation:  $CI=1000*a/(L*b)$ .

#### Identification of the Region of Interest (ROI), extraction, and correction of reflectance spectrum

The tools used in the image processing belong to the Spectronon Pro software (Resonon Inc., USA). The "selection of spectrally similar pixels" tool identified the ROI. Thus, the ROI was constituted by a set of pixels that are spectrally similar to the reference pixel (Figure 1a). This tool had a high performance in raw images due to no selection pixels with saturated reflectance. In intact samples, the tool was able to select a ROI with low spatial variation, avoiding the application of spatial correction methods that are used to overcoming the scattering of incident light on surface for intact fruits (Gómez-Sanchis et al., 2008; Peng and Lu, 2008). For half samples, the tool was able to select a ROI without considering different elements to the pulp like flavedo, albedo, seeds, etc. The raw mean reflectance spectrum of each sample was extracted by "mean spectrum" tool within the ROI (Figure 1b). Then, the correction of raw mean reflectance spectrum was performed to obtain the spectral signature of each sample (Figure 1c). For this, two images were acquired under the same setting conditions to image the samples. A dark image (~0% reflectance), for measuring dark current of the camera, was acquired with the light off and the camera lens completely covered by the cap. Using a white Teflon surface, a white image was obtained in order to detect the maximum reflectance (Resonon Inc. USA; ~99.9% reflectance). The corrected reflectance or relative reflectance ( $R$ ) was calculated with the following equation:  $R=[(R_0-B)/(W-B)]*100$ ; where  $R_0$  is the raw mean reflectance spectrum of the sample,  $B$  is the mean reflectance of the dark image, and  $W$  is the mean reflectance of the white image.

#### Modeling

Partial Least Squares Regression, a multivariable technique, was used to correlate the reference measurement of each quality attribute with the spectral information from orange fruit. This regression explains the descriptors through orthogonal factors also known as latent variables. The optimal number of latent variables applied to make the full model was determined by the minimum value of the average square error of prediction. The full model represented as follows  $Y=b.X+e$ .  $Y$  is the response matrix (1 x 60) of reference values obtained for quality attributes (TSS, pH, TA, TSS/TA,  $L^*$ ,  $a^*$ ,  $b^*$  or CI). The  $b$  is the matrix of regression coefficients (1 x 75). The  $X$  is the matrix of predictor variables constituted by the spectral signatures of the samples (75 x 60) and  $e$  is the matrix of residual information not explained by the model (1 x 60). This step was done in Matlab software (MathWorks Inc. USA). The model performance was evaluated on the calibration set using the coefficient of determination of calibration ( $R^2_c$ ) and Standard Error of Calibration (SEC), and on the prediction set using the coefficient of determination of prediction ( $R^2_p$ ) and Standard Error of Prediction (SEP) based on ElMasry et al. (2007). The selection of the optimal wavelengths that contain relevant information was made by identifying the highest local absolute value of the regression coefficients of the complete models. Simplified models were built by multiple linear regressions for their potential implementation in online applications, through multispectral imaging technologies (Liu et al., 2014). Additionally, a correlation analysis was carried out between the optimal wavelengths and the quality attributes for evaluating the regression coefficients of the simplified models (Xie et al., 2018). These steps were performed in Statistica 5.5 (Statsoft Inc. USA).

#### Results

The samples exhibited a widely range of variation of their quality attributes, since TSS/TA varied from 5.5 to 15.5 and CI varied from -3.3 to 2.5 (Table 1). The identification of the spectral peaks of the samples was carried out by a second derivative (Figure 2). Thus, peaks at 440, 472, 512, 584, 640, 816, and 976 nm were observed for intact and half samples, meanwhile, a peak at 672 nm was only detected in intact samples (Figure 2a).

The building of full models started with the study of number of latent variables (Figure 3). In general, for internal quality attributes, the exploration of latent variables for half samples showed a lower mean standard error of prediction than intact samples. The optimal number of

latent variables identified for intact and half samples was similar and relatively high (Figure 3a). It implied that the models were as complex for the intact samples as for half samples, confirmed through of a high number of optimal wavelengths for both type of samples (Figure 4a). For external quality attributes was identified a low optimal number of latent variables (Figure 3b), indicating the feasibility of the peel spectra to explain these attributes. The analysis of regression coefficients of the full models (Figure 4b) allowed the identification of a few optimal wavelengths to study in the model simplification.

The performance of the full models for internal quality

attributes, in terms of  $R^2_c$ ,  $R^2_p$ , SEC and SEP, confirmed that the models for half samples were better than that for intact samples (Table 2). The models for intact samples had relatively good performance in the calibration set ( $R^2_c > 0.57$ ); however, this behavior did not remain in the prediction set ( $R^2_p < 0.30$ ). Therefore, the prediction of internal quality attributes in intact orange was unviable using the built full model. Meanwhile, the models for half samples had a relatively good performance in the calibration set ( $R^2_c > 0.75$ ) and prediction set ( $R^2_p > 0.46$ ), being the highest predictive performance reached for TSS ( $R^2_c = 0.886$ ,  $SEC = 0.3$  and  $R^2_p = 0.757$ ,  $SEP = 0.5$ ).

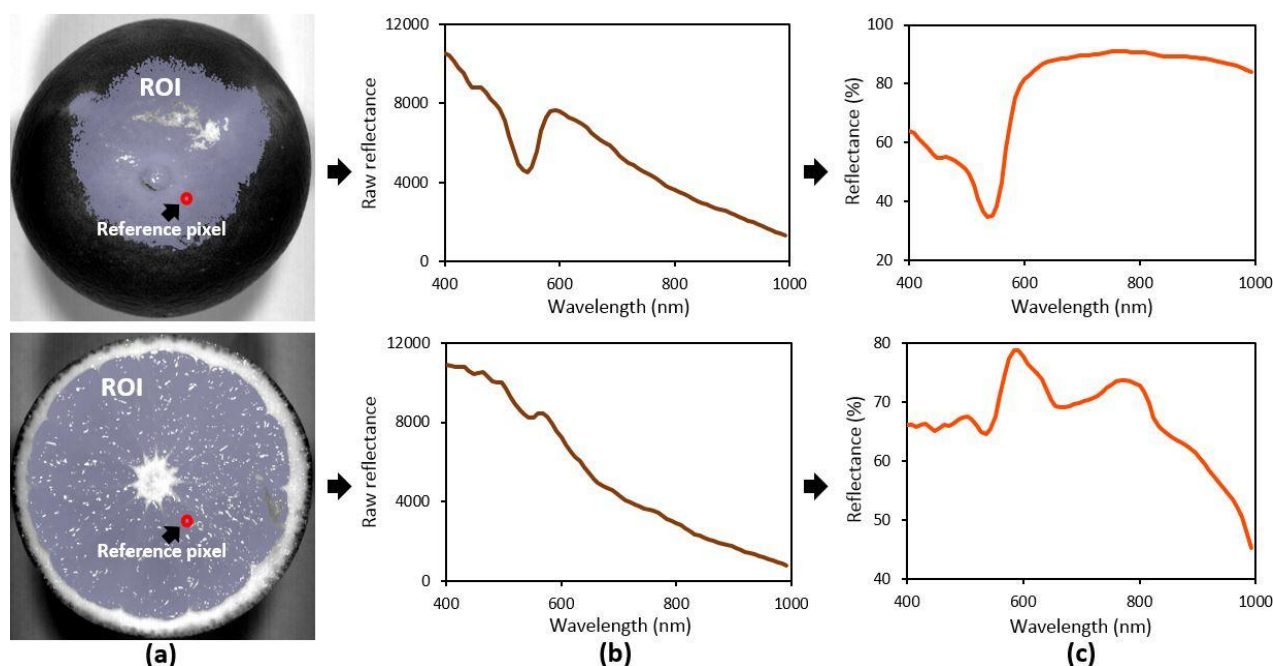


**Figure 1:** Main steps for image and spectra processing of orange fruit: (a) identification of the Region of Interest (ROI), (b) raw mean reflectance spectrum, and (c) corrected reflectance

**Table 1:** Internal and external quality attributes of orange fruit

| Quality attribute | Total (80 samples) |           | Calibration (60 samples) |           | Prediction (20 samples) |           |
|-------------------|--------------------|-----------|--------------------------|-----------|-------------------------|-----------|
|                   | Range              | Mean±SD   | Range                    | Mean±SD   | Range                   | Mean±SD   |
| TSS (%)           | 8.1-12.3           | 10.0±1.0  | 8.1-12.3                 | 10.0±1.0  | 8.9-12.0                | 10.0±0.9  |
| pH                | 3.14-3.83          | 3.53±0.16 | 3.14-3.83                | 3.53±0.17 | 3.34-3.75               | 3.53±0.13 |
| TA (%)            | 0.66-1.51          | 1.03±0.19 | 0.66-1.51                | 1.03±0.20 | 0.71-1.33               | 1.06±0.17 |
| TSS/TA            | 5.5-15.5           | 10.0±1.8  | 5.5-15.5                 | 10.0±1.8  | 6.7-13.4                | 9.8±1.9   |
| L*                | 54.8-70.0          | 65.8±3.6  | 54.8-69.9                | 66.2±3.2  | 54.9-70.0               | 64.5±4.4  |
| a*                | -8.2-10.6          | 4.5±4.2   | -8.2-10.6                | 4.8±3.7   | -8.2-10.1               | 3.8±5.4   |
| b*                | 44.5-63.8          | 59.3±4.2  | 44.5-63.8                | 59.6±3.6  | 44.6-63.7               | 58.3±5.7  |
| CI                | -3.3-2.5           | 1.1±1.2   | -3.2-2.5                 | 1.1±1.1   | -3.3-2.5                | 0.8±1.6   |

SD: Standard Deviation; TSS: Total Soluble Solids; TA: Titratable Acidity; CI: Color Index



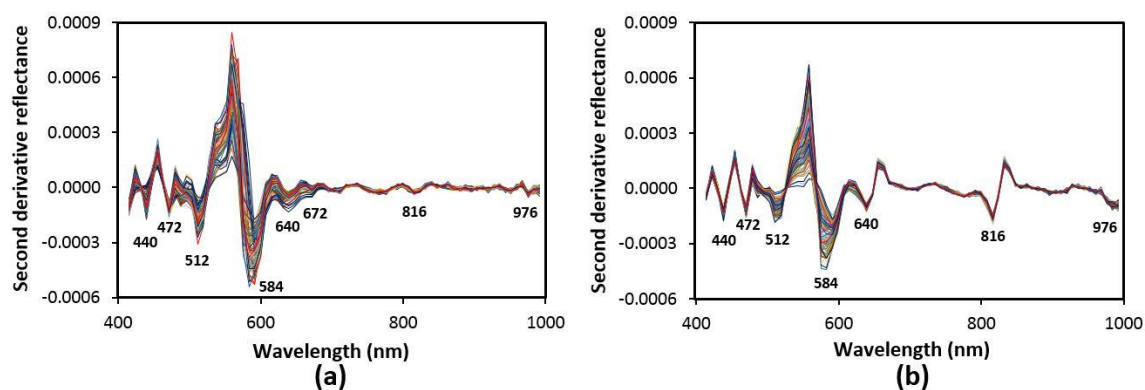


Figure 2: Second derivate spectra of orange fruit: (a) intact and (b) half samples

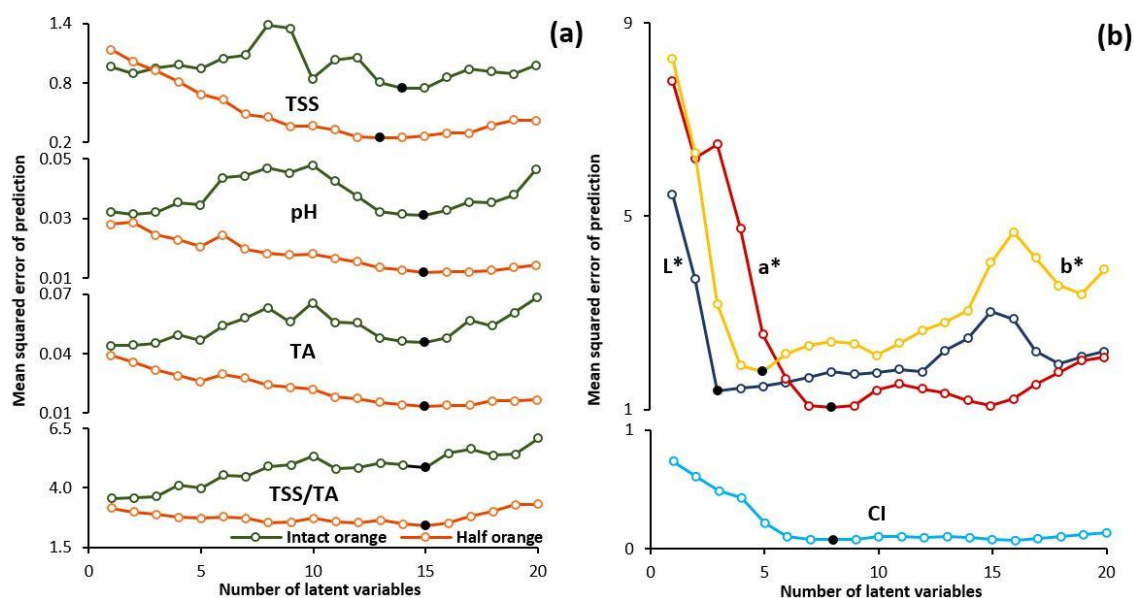


Figure 3: Mean Standard Error of Prediction (MSEP) of the models for predicting: (a) internal and (b) external quality attributes of orange fruit

Table 2: Performance of the full models for predicting quality attributes in orange fruit

| Quality attribute | Sample | Latent variables (No.) | Calibration |      | Prediction |      |         |
|-------------------|--------|------------------------|-------------|------|------------|------|---------|
|                   |        |                        | $R^2_c$     | SEC  | $R^2_p$    | SEP  | SEP (%) |
| TSS               | Intact | 14                     | 0.745       | 0.5  | 0.274      | 0.8  | 60      |
|                   | Half   | 13                     | 0.886       | 0.3  | 0.757      | 0.5  | 32      |
| pH                | Intact | 15                     | 0.620       | 0.11 | 0.180      | 0.16 | 59      |
|                   | Half   | 15                     | 0.858       | 0.07 | 0.553      | 0.10 | 35      |
| TA                | Intact | 15                     | 0.600       | 0.13 | 0.127      | 0.21 | 64      |
|                   | Half   | 15                     | 0.867       | 0.07 | 0.575      | 0.12 | 37      |
| TSS/TA            | Intact | 15                     | 0.579       | 1.2  | 0.297      | 2.2  | 54      |
|                   | Half   | 15                     | 0.750       | 0.9  | 0.465      | 1.6  | 45      |
| L*                | Intact | 3                      | 0.874       | 1.1  | 0.898      | 1.4  | 19      |
| a*                |        | 8                      | 0.953       | 0.8  | 0.952      | 1.2  | 13      |
| b*                |        | 5                      | 0.892       | 1.2  | 0.922      | 1.6  | 20      |
| CI                |        | 8                      | 0.957       | 0.2  | 0.972      | 0.3  | 12      |

$R^2_c$ : Coefficient of determination of calibration;  $R^2_p$ : Coefficient of determination of prediction; SEC: Standard Error of Calibration; SEP: Standard Error of Prediction; TSS: Total Soluble Solids; TA: Titratable Acidity; CI: Color Index

The high number of optimal wavelengths of the full models for internal quality attributes (Figure 4a) allowed an ineffective reduction of the spectral data for building simplified models with better performance (data not shown). It is worth mentioning that different spectral pre-processing such as Standard Normal Variate, Savitzky-Golay filter, first and second derivate, the transformation from reflectance to absorbance, and Kubelka-Munk function were also evaluated in the present study (data not

shown). However, no encouraging results were achieved when compared to those reached with reflectance data.

The full models for external quality attributes presented  $R^2_c$  and  $R^2_p$  values above 0.87 (Table 2). The SEP was higher than SEC for each color attribute; nonetheless, SEP values was up to 20%, which suggest that the models had a high performance, allowing the study of their simplification.

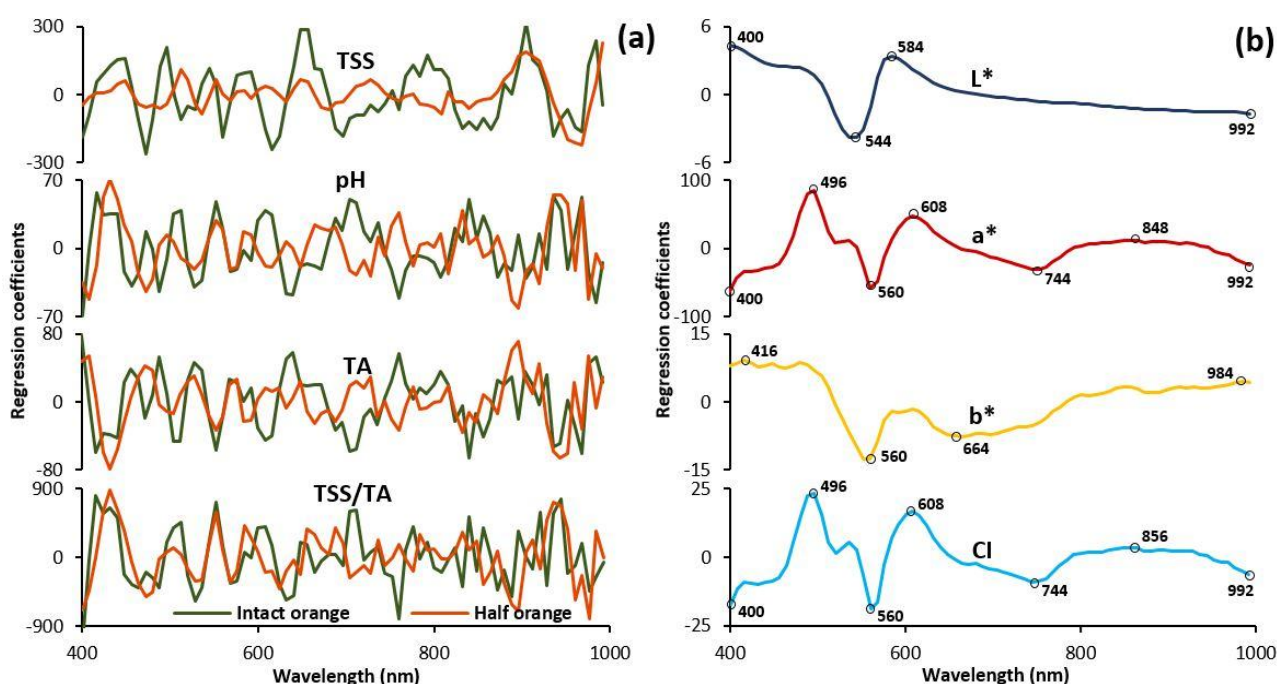


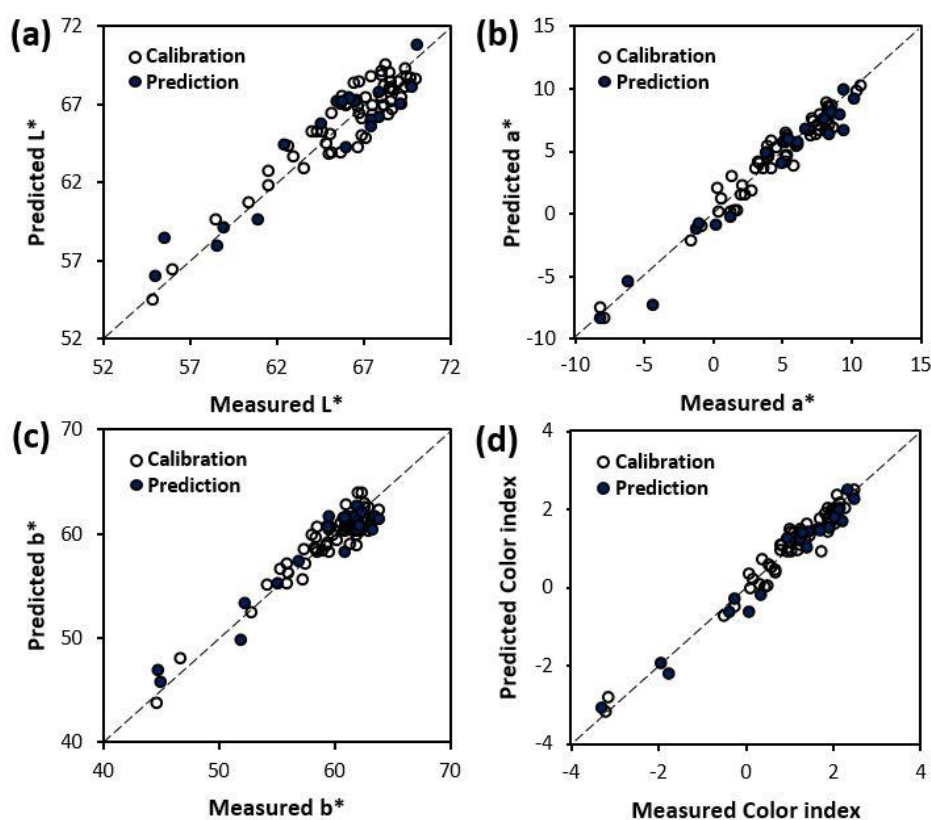
**Figure 4:** The regression coefficients of the full models for predicting: (a) internal as well as (b) external quality attributes of orange fruit

The analysis correlation of optimal wavelengths for external quality attributes (Table 3) showed that only the wavelengths between 400-600 nm had a high correlation ( $p < 0.05$ ), which could be related to the detection of carotenoids pigments in the samples. On the other hand, the analysis of multiple linear regression revealed that for  $L^*$  parameter, the most of the regression coefficients were significant, excepting for 400 nm ( $p > 0.05$ ). However, the use of the regression coefficient for 400 nm in the simplified model should be considered since the correlation

analysis evidenced that it is strongly correlated with the  $L^*$  parameter ( $p < 0.05$ ). Meanwhile, all the regression coefficients for  $a^*$  and  $b^*$  parameters and CI were highly significant ( $p < 0.05$ ). On the other hand, the evaluation of the simplified models for external quality attributes of orange fruit (Figure 5, Table 4) revealed that these presented a similar performance to their respective full models (Table 2). Therefore, the simplified models (Table 3) could be applied in the multispectral imaging systems.

**Table 3:** Correlation and multiple linear regression analysis for optimal wavelengths regarding external quality attributes of orange fruit

| Quality attribute | Wavelength (nm) | Correlation analysis |         |              | Multiple linear regression analysis |        |         |              |
|-------------------|-----------------|----------------------|---------|--------------|-------------------------------------|--------|---------|--------------|
|                   |                 | r value              | F value | Significance | Coefficients                        | Error  | t value | Significance |
| L*                | Interception    | -                    | -       | -            | 64.606                              | 1.463  | 44.17   | 0.000        |
|                   | 400             | 0.687                | 51.91   | 0.000        | 19.550                              | 11.376 | 1.72    | 0.091        |
|                   | 544             | 0.674                | 48.19   | 0.000        | -7.586                              | 2.451  | -3.10   | 0.003        |
|                   | 584             | 0.605                | 33.49   | 0.000        | 26.983                              | 13.309 | 2.03    | 0.047        |
|                   | 992             | 0.095                | 0.53    | 0.471        | -34.449                             | 3.628  | -9.50   | 0.000        |
| a*                | Interception    | -                    | -       | -            | 11.233                              | 1.689  | 6.65    | 0.000        |
|                   | 400             | 0.474                | 16.77   | 0.000        | -192.866                            | 15.379 | -12.54  | 0.000        |
|                   | 496             | 0.620                | 36.24   | 0.000        | 237.242                             | 18.057 | 13.14   | 0.000        |
|                   | 560             | 0.622                | 36.67   | 0.000        | -88.857                             | 9.358  | -9.50   | 0.000        |
|                   | 608             | 0.121                | 0.86    | 0.357        | 145.275                             | 19.159 | 7.58    | 0.000        |
|                   | 744             | 0.178                | 1.90    | 0.174        | -129.130                            | 24.281 | -5.32   | 0.000        |
|                   | 848             | 0.176                | 1.85    | 0.179        | 91.870                              | 28.762 | 3.19    | 0.002        |
| b*                | Interception    | -                    | -       | -            | 65.058                              | 1.578  | 41.22   | 0.000        |
|                   | 416             | 0.676                | 48.84   | 0.000        | 95.046                              | 6.860  | 13.86   | 0.000        |
|                   | 560             | 0.653                | 43.21   | 0.000        | -40.980                             | 4.488  | -9.13   | 0.000        |
|                   | 664             | 0.017                | 0.02    | 0.896        | -111.594                            | 12.037 | -9.27   | 0.000        |
|                   | 984             | 0.000                | 0.00    | 0.999        | 60.563                              | 9.885  | 6.13    | 0.000        |
| Color Index       | Interception    | -                    | -       | -            | 2.978                               | 0.468  | 6.36    | 0.000        |
|                   | 400             | 0.504                | 19.790  | 0.000        | -56.878                             | 4.262  | -13.35  | 0.000        |
|                   | 496             | 0.624                | 37.062  | 0.000        | 65.724                              | 5.012  | 13.11   | 0.000        |
|                   | 560             | 0.609                | 34.196  | 0.000        | -25.599                             | 2.598  | -9.86   | 0.000        |
|                   | 608             | 0.183                | 2.015   | 0.161        | 54.359                              | 5.305  | 10.25   | 0.000        |
|                   | 744             | 0.120                | 0.843   | 0.362        | -50.252                             | 6.519  | -7.71   | 0.000        |
|                   | 856             | 0.116                | 0.785   | 0.379        | 31.318                              | 7.929  | 3.95    | 0.000        |
|                   | 992             | 0.116                | 0.878   | 0.353        | -18.178                             | 4.369  | -4.16   | 0.000        |

**Figure 5:** Observed versus predicted values of external quality attributes using simplified models: (a) L\* parameter, (b) a\* parameter, (c) b\* parameter, and (d) color index

**Table 4:** Performance of the simplified models for predicting color components ( $L^*$ ,  $a^*$ , and  $b^*$ ) and color index in orange fruit

| Quality attribute | Number of wavelengths | Calibration |     | Prediction |     |         |
|-------------------|-----------------------|-------------|-----|------------|-----|---------|
|                   |                       | $R^2_c$     | SEC | $R^2_p$    | SEP | SEP (%) |
| $L^*$             | 4                     | 0.862       | 1.2 | 0.888      | 1.5 | 20      |
| $a^*$             | 7                     | 0.943       | 0.9 | 0.959      | 1.1 | 12      |
| $b^*$             | 4                     | 0.888       | 1.2 | 0.925      | 0.3 | 20      |
| CI                | 7                     | 0.947       | 0.2 | 0.974      | 0.3 | 9       |

$R^2_c$ : Coefficient of determination of calibration;  $R^2_p$ : Coefficient of determination in prediction; SEC: Standard Error of Calibration; SEP: Standard Error of Prediction

**Table 5:** Data comparison between this study and similar previous studies performed on prediction of quality attributes of orange fruit

| Quality attribute               | Mode        | Spectral range (nm) | Orange variety                                       | Method      | Best prediction level   | Reference                  |
|---------------------------------|-------------|---------------------|--|-------------|---|----------------------------|
| <i>Hyperspectral imaging</i>    |             |                     |  |             |   |                            |
| TSS                             | F           | 408-1117            | Nanfen   | PCA         | $R^2_p=0.996^*$   | Liu et al. (2007)          |
| TSS                             | R           | 400-1000            | Navel  | ANN         | $R^2_p=0.690^*$   | Guo et al. (2008)          |
| TSS<br>TSS/TA<br>CI             | R           | 400-1000            | Valencia   | PLSR        | $R^2_p=0.274$<br>$R^2_p=0.297$<br>$R^2_p=0.974$   | This study                 |
| <i>Spectroscopy</i>             |             |                     |  |             |   |                            |
| TSS<br>TA<br>pH                 | R           | 570-1850            | Valencia   | PLSR        | $R^2_c=0.913$<br>$R^2_c=0.637$<br>$R^2_c=0.499$   | Cayuela (2008)             |
| TSS<br>pH<br>TA<br>TSS/TA<br>CI | R           | 500-2300            | Sanguinelli,<br>Valencia,<br>Salustiana,<br>Navelate | PLSR        | $R^2_{cv}=0.83^*$<br>$R^2_{cv}=0.77^*$<br>$R^2_{cv}=0.69^*$<br>$R^2_{cv}=0.66^*$<br>$R^2_{cv}=0.76^*$ | Cayuela and Weiland (2010) |
| TSS                             | R           | 350-1800            | Navel  | PCA<br>BPNN | $R^2_p=0.83^*$  | Liu et al. (2010)          |
| CI<br>TSS<br>TA                 | R           | 780-2500            | Valencia   | PLSR        | $R^2_p=0.74^*$<br>$R^2_p=0.69^*$<br>$R^2_p=0.07^*$  | Magwaza et al. (2013)      |
| TSS                             | I<br>R<br>T | 200-1100            | Navel  | PLSR        | $R^2_{cv}=0.73^*$<br>$R^2_{cv}=0.76^*$<br>$R^2_{cv}=0.83^*$   | Wang et al. (2014)         |
| TSS<br>TA<br>TSS/TA             | R           | 450-2500            | Valencia   | PLSR        | $R^2_p=0.927$<br>$R^2_p=0.929$<br>$R^2_p=0.958$   | Ncama et al. (2017)        |

\*Converted from coefficient of correlation ( $r$ ) to coefficient of determination ( $R^2$ )

TSS: Total Soluble Solids; CI: Color Index; TA: Titratable Acidity; TSS/TA: Maturity index; R: Reflectance; I: Interactance; T: Transmittance; F: Fluorescence; PLSR: Partial Least Squares Regression; PCA: Principal Components Analysis; BPNN: Back Propagation Neural Network; ANN: Artificial Neural Network

## Discussion

The samples showed a widely range of variation in TSS, TA, and TSS/TA (Table 1) when compared to the measurements reported by Ramful et al. (2011). The color of the orange fruits varied from green to yellow (Table 1), as expected for Valencia variety. Thus, the variation of the quality attributes confirmed the suitability of the selected samples for building successful predictive models (ElMasry et al., 2013).

Statistical descriptors of the calibration set were similar to those obtained for total samples (Table 1), indicating

that the built models embraced the range of variation of total samples. Moreover, the calibration sets generally covered the ranges of the prediction sets, suggesting that the division of the sample was adequate (Dong et al., 2016).

The intact and half samples showed peaks from 440 nm to 640 nm, which could be attributed to carotenoid pigments observed at 435 nm (Huang et al., 2014), 450 nm, 580 nm (Munera et al., 2017) and in the range of 400-600 nm (Munera et al., 2018) in the other studies. The



intact samples showed a peak at 672 nm, which could be related to chlorophyll pigment reported at 673 nm (Zhu et al., 2017), 675 nm (Peng and Lu, 2008), and 680 nm (Munera et al., 2017). Other peaks were observed in intact and half samples at 816 and 976 nm. The peak at 816 nm could be associated with acids and sugars since acids were detected at 800 nm (Munera et al., 2018), and sugars were identified at 835 nm (Zhu et al., 2017) and 840 nm (Xie et al., 2018). The peak detected at 976 nm could be related to water and sugars since water was detected at 960 nm (ElMasry et al., 2007), 970 nm (Munera et al., 2018), and 976 nm (Zhu et al., 2017). On the other hand, water and sugars were reported at 970 nm (Teerachaichayut and Ho, 2017) and in the ranges of 960-980 nm (Dong et al., 2016) and 970-980 nm (Leiva-Valenzuela et al., 2013). In particular, the last peaks were difficult to observe in the intact samples when compared to half samples. This behavior was expected as the compositional and structural differences between the peel and pulp result in some difficulty in the extraction of spectral data during hyperspectral imaging (Wang et al., 2014).

The full models for internal quality attributes reached unacceptable predictive performance (Table 2) with exception of the full model for TSS in half samples. The study of simplification of these models suggested the loss of fundamental information and could be the reason why some authors had no reports of the simplified models recommending the use of full models for industries (Rodríguez-Pulido et al., 2014). In that sense, the full model for TSS in half samples could be used as a complementary assessment to traditional methods in a noncontact and rapid way (Ma et al., 2018). In further works, the building of simplified models for TSS and other internal quality attributes in multispectral imaging technologies should involve the exploration of the spectral region of near infrared (>1000 nm). It provides enhanced sensitivity to internal composition when compared to the visible-near infrared region (400-1000 nm; Ma et al., 2018).

Hyperspectral imaging studies in orange fruit were focused on the prediction of TSS (Table 5). The  $R^2_p$  for TSS in intact orange fruit obtained in this study (0.274) was lower than those reported for "Navel" orange by hyperspectral reflectance imaging (0.691; Guo et al., 2008) and for "Nanfen" orange fruit by hyperspectral laser-induced fluorescence imaging (0.996; Liu et al., 2007). This difference could be attributed to the fruit variety and the hyperspectral imaging technique or system setting. Hence, calibration of models by artificial neural networks could be time-consuming and impractical for recalibrations works and that laser-induced fluorescence could cause damage to fruit (Liu et al., 2007), compromising the practical application of the results.

Spectroscopy studies in orange fruit were focused on predicting TSS, pH, TA, TSS/TA, and CI using mainly the reflectance mode (Table 5). In general, good predicting levels for internal quality attributes were reached by spectroscopy technique, which could be attributed to the use of near infrared region (>1000 nm). The prediction level of CI was better for hyperspectral imaging ( $R^2_p=0.974$ ) when compared to the reached maximum level by spectroscopy ( $R^2_{cv}=0.76$ ; Cayuela and Weiland, 2010), which demonstrated that the spectral region of 400-1000 nm allows the obtaining of high-quality information related to color of orange fruit.

## Conclusion

Hyperspectral reflectance imaging technique (400-1000 nm) can be applied to predicting TSS in half orange fruit and color ( $L^*$ ,  $a^*$ , and  $b^*$  parameters; and CI) in intact orange fruit, in an objective and noncontact way. Full models for predicting internal quality attributes in intact orange fruit (TSS, pH, TA, TSS/TA) had low performance. The full and simplified models for external quality attributes had high performance, suggesting that simplified models could be applied in a multispectral reflectance imaging system for predicting color of orange fruit. The results of this study can be used as a reference in the implementation of multispectral technologies for quality assurance of orange fruit. Further improvements in the prediction of internal quality attributes in intact orange fruit could be achieved in future studies by a different spectral region (>1000 nm).

## Author contributions

All the authors contributed equally to experimental design, data collection, data analysis, and paper writing. All the authors read and approved the final manuscript.

## Conflicts of interest

All the authors declared that they have no conflict of interest.

## Acknowledgements

The authors thank the Universidad Nacional de Trujillo - UNT (PIC2-2013/UNT) by the financial support. The authors would also like to thank Michael James Stablein of the University of Illinois Urbana-Champaign for his translation and review services of this work.

## References

- Aredo V., Velásquez L., Siche R. (2017). Prediction of beef marbling using Hyperspectral Imaging (HSI) and Partial Least Squares Regression (PLSR). *Scientia Agropecuaria*. 8: 169-174. [DOI: 10.17268/sci.agropecu.2017.02.09]
- Association of Official Analytical Chemists (AOAC). (2005). Official methods of analysis. AOAC International, Gaithersburg.
- Barreto A., Cruz-Tirado J.P., Siche R., Quevedo R. (2018). Determination of starch content in adulterated fresh cheese using hyperspectral imaging. *Food Bioscience*. 21: 14-19. [DOI: 10.1016/j.fbio.2017.10.009]
- Cayuela J.A. (2008). Vis/NIR soluble solids prediction in intact oranges (*Citrus sinensis* L.) cv. Valencia Late by reflectance. *Postharvest Biology and Technology*. 47: 75-80. [DOI: 10.1016/j.postharvbio.2007.06.005]
- Cayuela J.A., Weiland C. (2010). Intact orange quality prediction with two portable NIR spectrometers. *Postharvest Biology and Technology*. 58: 113-120. [DOI: 10.1016/j.postharvbio.2010.06.001]
- Dong J., Guo W., Wang Z., Liu D., Zhao F. (2016). Nondestructive determination of soluble solids content of 'Fuji' Apples produced in different areas and bagged with different materials during ripening. *Food Analytical Methods*. 9: 1087-1095. [DOI: 10.1007/s12161-015-0278-4]
- ElMasry G., Sun D.W., Allen P. (2013). Chemical-free assessment and mapping of major constituents in beef using hyperspectral imaging. *Journal of Food Engineering*. 117: 235-246. [DOI: 10.1016/j.jfoodeng.2013.02.016]
- ElMasry G., Wang N., ElSayed A., Ngadi M. (2007). Hyperspectral imaging for nondestructive determination of some quality attributes for strawberry. *Journal of Food Engineering*. 81: 98-107. [DOI: 10.1016/j.jfoodeng.2006.10.016]
- Folch-Fortuny A., Prats-Montalbán J.M., Cubero S., Blasco J., Ferrer A. (2016). VIS/NIR hyperspectral imaging and N-way PLS-DA models for detection of decay lesions in citrus fruits. *Chemometrics and Intelligent Laboratory Systems*. 156: 241-248. [DOI: 10.1016/j.chemolab.2016.05.005]
- Gómez-Sanchis J., Moltó E., Camps-Valls G., Gómez-Chova L., Aleixos N., Blasco J. (2008). Automatic correction of the effects of the light source on spherical objects. An application to the analysis of hyperspectral images of citrus fruits. *Journal of Food Engineering*. 85: 191-200. [DOI: 10.1016/j.jfoodeng.2007.06.036]
- Guo E., Liu M., Zhao J., Chen Q. (2008). Nondestructive detection of sugar content on navel orange with hyperspectral imaging. *Transactions of the Chinese Society for Agricultural Machinery*. 39: 91-93.
- Guo W., Zhao F., Dong J. (2016). Nondestructive measurement of soluble solids content of kiwifruits using near-infrared hyperspectral imaging. *Food Analytical Methods*. 9: 38-47. [DOI: 10.1007/s12161-015-0165-z]
- Huang M., Wang Q., Zhang M., Zhu Q. (2014). Prediction of color and moisture content for vegetable soybean during drying using hyperspectral imaging technology. *Journal of Food Engineering*. 128: 24-30. [DOI: 10.1016/j.jfoodeng.2013.12.008]
- Leiva-Valenzuela G.A., Lu R., Aguilera J.M. (2013). Prediction of firmness and soluble solids content of blueberries using hyperspectral reflectance imaging. *Journal of Food Engineering*. 115: 91-98. [DOI: 10.1016/j.jfoodeng.2012.10.001]
- Li J., Rao X., Ying Y. (2011). Detection of common defects on oranges using hyperspectral reflectance imaging. *Computers and Electronics in Agriculture*. 78: 38-48. [DOI: 10.1016/j.compag.2011.05.010]
- Liu Y., Sun X., Ouyang A. (2010). Nondestructive measurement of soluble solid content of navel orange fruit by visible-NIR spectrometric technique with PLSR and PCA-BPNN. *LWT-Food Science and Technology*. 43: 602-607. [DOI: 10.1016/j.lwt.2009.10.008]
- Liu D., Sun D.W., Zeng X.A. (2014). Recent advances in wavelength selection techniques for hyperspectral image processing in the food industry. *Food and Bioprocess Technology*. 7: 307-323. [DOI: 10.1007/s11947-013-1193-6]
- Liu M., Zhang L., Guo E. (2007). Hyperspectral laser-induced fluorescence imaging for nondestructive assessing soluble solids content of orange. In: Li D. (Editor) Computer and computing technologies in agriculture. Volume I. Springer, Boston, MA. pp. 51-59. [DOI: 10.1007/978-0-387-77251-6\_7]
- Ma T., Li X., Inagaki T., Yang H., Tsuchikawa S. (2018). Noncontact evaluation of soluble solids content in apples by near-infrared hyperspectral imaging. *Journal of Food Engineering*. 224: 53-61. [DOI: 10.1016/j.jfoodeng.2017.12.028]
- Magwaza L.S., Opara U.L., Terry L.A., Landahl S., Cronje P.J.R., Nieuwoudt H.H., Hanssens A., Saeys W., Nicolai B.M. (2013). Evaluation of Fourier transform-NIR spectroscopy for integrated external and internal quality assessment of Valencia oranges. *Journal of Food Composition and Analysis*. 31: 144-154. [DOI: 10.1016/j.jfca.2013.05.007]
- Munera S., Amigo J.M., Aleixos N., Talens P., Cubero S., Blasco J. (2018). Potential of VIS-NIR hyperspectral imaging and chemometric methods to identify similar cultivars of nectarine. *Food Control*. 86: 1-10. [DOI: 10.1016/j.foodcont.2017.10.037]
- Munera S., Besada C., Aleixos N., Talens P., Salvador A., Sun D.W., Cubero S., Blasco J. (2017). Non-destructive assessment of the internal quality of intact persimmon using colour and VIS/NIR hyperspectral imaging. *LWT-Food Science and Technology*. 77: 241-248. [DOI: 10.1016/j.lwt.2016.11.063]
- Ncama K., Opara U.L., Tesfay S.Z., Fawole O.A., Magwaza L.S. (2017). Application of Vis/NIR spectroscopy for predicting sweetness and flavour parameters of 'Valencia' orange (*Citrus sinensis*) and 'Star Ruby' grapefruit (*Citrus x paradisi* Macfad). *Journal of Food Engineering*. 193: 86-94. [DOI: 10.1016/j.jfoodeng.2016.08.015]
- Orrillo I., Cruz-Tirado J.P., Cardenas A., Oruna M., Carnero A., Barbin D.F., Siche R. (2019). Hyperspectral imaging as a powerful tool for identification of papaya seeds in black pepper. *Food Control*. 101: 45-52. [DOI: 10.1016/j.foodcont.2019.02.036]
- Peng Y., Lu R. (2008). Analysis of spatially resolved hyperspectral scattering images for assessing apple fruit firmness and soluble solids content. *Postharvest Biology and Technology*. 48: 52-62. [DOI: 10.1016/j.postharvbio.2007.09.019]
- Ramful D., Tarnus E., Aruoma O.I., Bourdon E., Bahorun T. (2011). Polyphenol composition, vitamin C content and antioxidant capacity of Mauritian citrus fruit pulps. *Food Research International*. 44: 2088-2099. [DOI: 10.1016/j.foodres.2011.03.056]
- Rodríguez-Pulido F.J., Hernández-Hierro J.M., Nogales-Bueno J., Gordillo B., González-Miret M.L., Heredia F.J. (2014). A novel method for evaluating flavanols in grape seeds by near infrared hyperspectral imaging. *Talanta*. 122: 145-150. [DOI: 10.1016/j.talanta.2014.01.044]
- Saldaña E., Siche R., Castro W., Huamán R., Quevedo R. (2014). Measurement parameter of color on yacon (*Smallanthus sonchifolius*) slices using a computer vision system. *LWT-Food Science and Technology*. 59: 1220-1226. [DOI: 10.1016/j.lwt.2014.06.037]
- Siche R., Vejarano R., Aredo V., Velasquez L., Saldaña E., Quevedo R. (2016). Evaluation of food quality and safety with hyperspectral imaging (HSI). *Food Engineering Reviews*. 8: 306-322. [DOI: 10.1007/s12393-015-9137-8]
- Teerachaichayut S., Ho H.T. (2017). Non-destructive prediction of total soluble solids, titratable acidity and maturity index of limes by near infrared hyperspectral imaging. *Postharvest Biology and Technology*. 133: 20-25. [DOI: 10.1016/j.postharvbio.2017.07.005]
- United States Department of Agriculture (USDA). (2019). Citrus: world markets and trade. USDA. Foreign Agricultural Service. <https://apps.fas.usda.gov/psdonline/circulars/citrus.pdf>. Accessed 30 July 2019.
- Vejarano R., Siche R., Tesfaye W. (2017). Evaluation of biological contaminants in foods by hyperspectral imaging: a review.

- International Journal of Food Properties*. 20: 1264-1297. [DOI: 10.1080/10942912.2017.1338729]
- Velásquez L., Cruz-Tirado J.P., Siche R., Quevedo R. (2017). An application based on the decision tree to classify the marbling of beef by hyperspectral imaging. *Meat Science*. 133: 43-50. [DOI: 10.1016/j.meatsci.2017.06.002]
- Wang A., Hu D., Xie L. (2014). Comparison of detection modes in terms of the necessity of visible region (VIS) and influence of the peel on soluble solids content (SSC) determination of navel orange using VIS-SWNIR spectroscopy. *Journal of Food Engineering*. 126: 126-132. [DOI: 10.1016/j.jfoodeng.2013.11.011]
- Wei X., He J.C., Ye D.P., Jie D.F. (2017). Navel orange maturity classification by multispectral indexes based on hyperspectral diffuse transmittance imaging. *Journal of Food Quality*. 2017: 1-7. [DOI: 10.1155/2017/1023498]
- Xie C., Chu B., He Y. (2018). Prediction of banana color and firmness using a novel wavelengths selection method of hyperspectral imaging. *Food Chemistry*. 245: 132-140. [DOI: 10.1016/j.foodchem.2017.10.079]
- Yin S., Bi X., Niu Y., Gu X., Xiao Y. (2017). Hyperspectral classification for identifying decayed oranges infected by fungi. *Emirates Journal of Food and Agriculture*. 29: 601-609. [DOI: 10.9755/ejfa.2017-05-1074]
- Zhang D., Xu Y., Huang W., Tian X., Xia Y., Xu L., Fan S. (2019). Nondestructive measurement of soluble solids content in apple using near infrared hyperspectral imaging coupled with wavelength selection algorithm. *Infrared Physics and Technology*. 98: 297-304. [DOI: 10.1016/j.infrared.2019.03.026]
- Zhu H., Chu B., Fan Y., Tao X., Yin W., He Y. (2017). Hyperspectral imaging for predicting the internal quality of kiwifruits based on variable selection algorithms and chemometric models. *Scientific Reports*. 7: 7845. [DOI: 10.1038/s41598-017-08509-6]